

Temperature Dependence of
 $\text{Cu}_{3-x}(\text{Sb}_{1-y}\text{M}_y)\text{S}_4$ (M = Sn, Ge)
Resistivity and Thermopower

by Joshua Mutch

*A thesis submitted in partial fulfillment of
the requirements for the degree of*

Bachelor of Science in Physics

Oregon State University
Corvallis, Oregon

May, 2015

Advisor: Dr. Janet Tate

Acknowledgements

Many thanks to the physics community at Oregon State University. First, thanks to Dr. Janet Tate for her guidance, teaching, and mentoring. Dr. Robert Kokenyesi, for providing the bulk Cu_4SbS_4 samples. Mark Warner, for electrical guidance and advice. Larry Antal, for machining the current experimental setup and useful insights and conversations. Previous year's undergraduate students Rodney Snyder, Aaron Kratzer, and Daniel Speer, for instruction on lab equipment and much more. Current graduate students Chris Reidy, James Haggerty, Bethany Matthews, and Greg Angelos, for many helpful conversations. Current undergraduate seniors Scott Hutchings and Alex Poff, for helpful conversations. Current undergraduate juniors Katie Banowetz and Josh Stahly, for continuity of the laboratory group. Thanks as well to Dr. Doug Keszler, Dr. John Wager, Greg Angelos, and Jaesoek Heo for large group collaboration meetings.

Funding for work done during the summer of 2014 was provided by the SURE program at OSU. Thanks to Dr. Kevin Ahern and Claire Colvin for their participation in the program.

Abstract

An experimental apparatus is modified to allow measurements of the Seebeck coefficient and resistivity to be taken simultaneously. This apparatus is designed for bulk and thin film samples between temperatures of 10 K and 300 K. The apparatus is constructed such that these simultaneous measurements do not interfere with each other, minimizing experimental time and overhead associated with each measurement. A COMSOL Multiphysics software model of the current experimental apparatus is constructed. The software model uses the finite element method to solve the heat transfer equation, and indicates that the apparatus can maintain thermal conditions for non-interference between the two measurements. A temperature difference across the sample can be generated to measure the Seebeck coefficient, while the resistivity measurement is performed along an isothermal contour.

Using this apparatus, measurements on Cu_3SbS_4 are made to determine the potential of Cu_3SbS_4 as a thermoelectric material. Thermoelectric materials are an active area of research today, with applications in cooling and converting waste heat to useable energy. The resistivity and Seebeck coefficient of bulk Cu_3SbS_4 and doped variants are measured for temperatures between 10 K and 300 K. Bulk Cu_3SbS_4 is found to have a room temperature Seebeck coefficient of $800 \mu\text{V/K}$, and a resistivity of $4.5 \Omega \text{ cm}$. The resistivity has semiconductor-like behavior, with an activation energy that increases with temperature, opposite to the theoretical prediction. The Seebeck coefficient increases with temperature until 130 K, then decreases with temperature. At temperatures above 130 K, the Seebeck coefficient decreases with increasing temperature, but is not proportional to $1/T$. Jonker analysis of the Seebeck coefficient and electrical conductivity does not match a theoretical k/e slope.

Doping with 1% Sn reduces the magnitude of the Seebeck coefficient by $\sim 75\%$, with even larger reductions for 5% Sn and 5% Ge doping. Doping with 3% copper vacancies results in a relatively small, $\sim 20\%$ reduction in the magnitude of the Seebeck coefficient. The resistivity of the sample with 3% copper vacancies has semiconductor-like behavior, while the samples doped with 5% Sn and Ge have a metallic-like resistivity. Cu_3SbS_4 doped with 5% Ge displays the highest power factor of the samples measured. $PF = 1.04 \times 10^{-4} \text{ W/K}^2\text{m}$ is measured for the 5% Ge sample at 300 K.

Table of Contents

1. Introduction.....	1
Background.....	1
Applications.....	1
Benchmarks for Efficiency.....	1
Current Research.....	1
Summary and goals.....	2
2. Theory.....	3
Basics of Resistivity.....	3
Resistivity temperature dependence of semiconductors.....	3
Resistivity temperature dependence of metals.....	5
Seebeck Effect - Metals and Semiconductors.....	6
Goldsmid-Sharp – Seebeck Coefficient Analysis.....	7
Seebeck Coefficient Temperature Dependence - Summary.....	8
Jonker Plots – Thermopower and Resistivity comparison.....	8
3. Materials.....	10
<i>p</i> Type and <i>n</i> Type Doping.....	10
Cu ₃ Sb _{1-y} M _y S ₄ (M=Sn, Ge).....	10
Indium Tin Oxide (ITO).....	11
Bismuth Telluride.....	11
4. Methods.....	12
Cryogenic Setup and Methodology.....	12
Inline Four Probe Resistivity Measurement.....	14
Seebeck Coefficient Measurement.....	15
Simultaneous resistivity & thermopower measurement.....	17
COMSOL Modeling.....	18
4. Results.....	21
Indium Tin Oxide.....	21
Cu ₃ SbS ₄	21
6. Discussion.....	27
7. Conclusion.....	29
8. Appendices.....	30

Appendix 1: Cryogenic properties used in COMSOL model.....	30
Appendix 2: Cryostat Warming Guidelines.....	32
9. Bibliography	34

List of Figures

Figure 2-1: Band structure for an n type semiconductor	4
Figure 2-2: Carrier density temperature dependence of extrinsic semiconductor [5, pg 584]	5
Figure 2-3: Error of Goldsmid-Sharp band gap approximation as a function of mobility and effective mass ratio of charge carriers.	8
Figure 2-4: Qualitative power Jonker plot and power factor curve for non-degenerate semiconductors.	9
Figure 3-1: Crystal Structure of Cu_3SbS_4	10
Figure 4-1: Cold head apparatus with experimental setup shielded by the inner casing. Location of Si Diode and Type K thermocouple shown on the right.	12
Figure 4-2: Flow diagram for performing temperature dependent thermopower measurements. Times shown can be increased to increase quality of measurements, or decreased to hasten the experiment. Not shown: resistivity data is logged simultaneous to this process.	14
Figure 4-3: Four probe contact pins and material (left) and equivalent circuit diagram (right) ...	15
Figure 4-4: Experimental setup. Side view (left) and top down view (right)	16
Figure 4-5: Schematic of measuring apparatus (left). Dataset for Cu_3SbS_4 (right)	17
Figure 4-6: Previous (left) and current (right) experimental setup	17
Figure 4-7: COMSOL heat transfer model of experimental setup at 20 K (left) and 300 K (right). See Appendix 1 for summary of cryogenic material properties and assumptions made in the COMSOL model.	18
Figure 4-8: Heating response of the experimental apparatus, simulated with COMSOL Multiphysics software. The density of silicon (2330 kg/m^3) was assumed to calculate specific heat corresponding to the labeled thermal diffusivity value.	20
Figure 4-1: Transport measurements for two difference samples of thin-film ITO, fabricated under different conditions.	21
Figure 4-2: Bulk Cu_3SbS_4 resistivity measurements (left) and thermopower measurements (right)	22
Figure 4-3: Cu_3SbS_4 Jonker analysis at room temperature (left) and 100 K (right). A line with a slope of $-k/e$ and an arbitrary intercept has been fitted in each graph	23
Figure 4-4: Activation energy analysis for Cu_3SbS_4 . Pure sample (upper left), Cu=2.9 (top right), and 1% Sn sample (bottom left).	24
Figure 8-1: Type K temperature and silicon diode temperature of the experimental setup as the cryostat is warmed. At ~400 minutes, the LabView program halted while it prompted the user to turn off the cryopump. At ~600 minutes, the cryostat warmed with the cryopump off. Below ~400 minutes, the incremental adjustment of the temperature set point can be seen. Zeros seen in this graph are a result of dropped communication packets between the Lakeshore 320 and the Labview program.	32
Figure 8-2: The voltage measured by the difference thermocouple as a function of time.	33

1. Introduction

Background

The discovery of the phenomenon of thermoelectricity dates back to the nineteenth century, when two important discoveries were made. The first was made by Johann Seebeck, who discovered that a temperature difference across two ends of a material creates a voltage across the material. The second discovery was made by Jean Peltier, who discovered that current flowing through a junction of two different materials results in heat added or removed from the system. These two effects form the basis for many applications of thermoelectric devices.

Applications

Thermoelectric materials have applications in power generation and cooling. In power generation, a thermoelectric device can be used to convert a temperature difference to usable power. In cooling, driving a current through a thermoelectric device can cool the device. Internal combustion engines often operate at efficiencies less than 40%, with the bulk of the wasted energy dissipated as excess heat. This market alone creates an energy savings opportunity for efficient thermoelectric devices to capture a portion of this energy. Thermoelectric coolers also present a more environmental friendly cooling process compared to traditional thermodynamic refrigeration methods. Conventional refrigeration processes often rely on refrigerants containing environmentally unfriendly chlorofluorocarbons.

Benchmarks for Efficiency

The market for thermoelectric devices requires engineering attention to maximize efficiency. Factors such as temperature, the temperature difference between thermal reservoirs, and system's thermal resistance impact the efficiency of thermoelectric devices [8]. The figure of merit, or ZT (Equation 1), is commonly used to gauge the efficiency of a thermoelectric device. A common benchmark is $ZT=1$, which indicates a material that shows promise as a thermoelectric device. There is no theoretical upper limit on the value of ZT , although recent research has seen no large improvements in the value of ZT .

$$ZT = \frac{S^2 \sigma T}{K} \quad 1$$

In Equation 1 above, S is the Seebeck coefficient, σ the electrical conductivity, T the absolute temperature, and K the thermal conductivity.

Current Research

Research on improving the ZT of a material often falls into one of two main categories: reducing the thermal conductivity, or increasing the power factor (PF). This paper will focus on the latter. The Seebeck coefficient and electrical resistivity is measured for Cu_3SbS_4 and variants thereof, and the corresponding PFs are analyzed to determine if these materials show promise as thermoelectric materials. The PF appears in the figure of merit, and is defined in Equation 2 below:

$$PF = S^2 \sigma \quad 2$$

Chalcogenides are a material group that show promise as potential thermoelectric devices. Chalcogenides are compounds with at least one group 16, non-oxygen element. Because of the consistent electronegativity across the group 16 elements, many chalcogenides show consistent energy gaps that are within target regions for thermoelectric devices [10]. One of the leading thermoelectric materials is Bi_2Te_3 , which has a PF of $4.8 \times 10^{-3} \text{ W/mK}^2$, and a ZT of ~ 1 [11].

Summary and goals

This paper focuses on measuring the electrical transport properties to calculate the PF. The Seebeck coefficient (the magnitude of which is often referred to as thermopower) and electrical conductivity are discussed and measured for Cu_3SbS_4 . The temperature dependence of these properties can provide insight into the band structure of a material. The temperature dependence of the Seebeck coefficient and electrical resistivity is different between metals and semiconductors. The resistivity and Seebeck coefficient for metals usually increase linearly with temperature, while these properties usually display a $1/T$ trend for semiconductors. This $1/T$ trend is not always the case for the Seebeck coefficient in semiconductors, and will be further discussed in the Theory section.

The resistivity and thermopower for indium tin oxide (ITO) and Cu_3SbS_4 are measured for temperatures between 10 K and 300 K, and the results discussed. The experimental setup was recently modified to allow simultaneous measurements of these properties. A COMSOL Multiphysics software model of the experimental setup simulates heat transfer to examine the accuracy of the measurements.

The Theory section examines the basic principles governing resistivity and thermopower, specifically examining the difference between semiconductors and metals. Jonker analysis is introduced in the Theory section, along with the Goldsmid-Sharp band gap estimation method. A Materials section introduces the motivation for studying Cu_3SbS_4 , and introduces materials used as benchmarks. Next, the Methods section details the methodology used to measure resistivity and thermopower in a low temperature regime, and examines the COMSOL model of the system. The Results section shows measurement results for ITO and Cu_3SbS_4 , which are further discussed in the Discussion section. Finally, the Conclusion section summarizes the findings and proposes possible next steps in the evolution of experiment.

2. Theory

Basics of Resistivity

Electricity conductivity (σ) is an intrinsic property of a material that dictates how much current will flow through a material given an applied electric field. Resistivity (ρ) is the inverse of conductivity. The factors that determine a material's resistivity are shown in Equation 3 below.

$$\sigma = \frac{1}{\rho} = e(n\mu_n + p\mu_p) \quad 3$$

where e is the fundamental charge, n and p are the carrier concentrations for negative and positive charge carriers, respectively, and μ is the mobility. Often, a material is dominated by either positive or negative charge carriers. For the case of a material dominated by n type carriers, Equation 3 becomes:

$$\sigma = \frac{1}{\rho} = n\mu e \quad 4$$

It is understood that μ in Equation 4 refers to the mobility of the dominant carriers.

To examine how resistivity depends on temperature, both the temperature dependence of carrier concentration and mobility are analyzed. Both these properties vary with temperature. However, the temperature dependence of these properties is different between metals and semiconductors. For metals, the carrier concentration changes very little as a function of temperature, and variations in mobility dominate the temperature dependence of conductivity. For semiconductors, the variation in mobility is outweighed by dramatic changes in carrier concentration. The change in carrier concentration for a semiconductor spans orders of magnitude. The temperature dependence of semiconductors and metals will be examined in more detail in the following sections.

Resistivity temperature dependence of semiconductors

To examine the temperature dependence of resistivity for semiconductors, it is approximated that the resistivity is primarily dependent on carrier concentration rather than mobility. This approximation is justified by examining experimental evidence for the temperature dependence of mobility. Experimental evidence shows that, for germanium and silicon, mobility depends on temperature raised to a power, from T^{-1} to $T^{-2.3}$ [16]. Since it is shown in Equation 6 that carrier concentration depends on an exponential of temperature, the variations in carrier concentration outweigh variations in mobility. Equation 5 highlights the approximation that the resistivity only depends on the carrier concentration.

$$\rho(T) \propto \frac{1}{n(T)} \quad 5$$

It is noted in Equation 5 that an n type semiconductor is assumed. The same analysis holds true for p type semiconductors, but only the n type is analyzed for simplicity. To analyze p type materials, the analysis on the following pages would be the same, but carrier promotions from

the valence band to the impurity band would be considered rather than carrier promotions from the impurity band to the conduction band. To analyze the n type materials, the band structure of an n type semiconductor is shown in Figure 2-1.

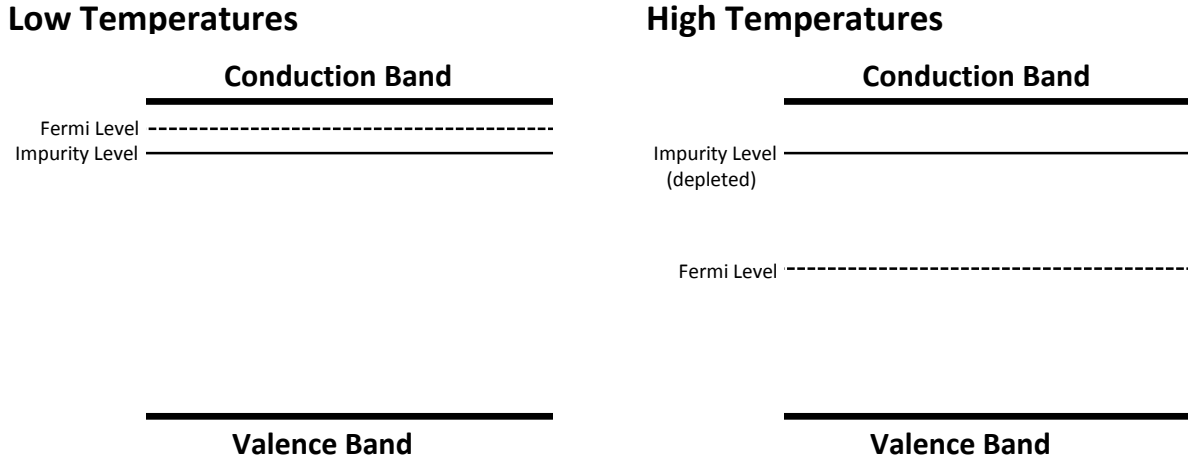


Figure 2-1: Band structure for an n type semiconductor

The Fermi level is defined to be the energy difference between the highest occupied state and the lowest unoccupied state. At 0 K, the impurity level is occupied and the conduction band is fully unoccupied. The Fermi level in this scenario is half way between the impurity level and the conduction band. At higher temperatures, when the conduction band is depleted, the Fermi level drops to approximately half way between the conduction band and the valence band.

Every electron promoted from the valence band to the conduction band produces a negative charge carrier in the conduction band and a positive charge carrier in the valence band. Considering only these carrier promotions, the carrier density is given by Equation 6 [1, pg 96].

$$n(T) \propto e^{-E_G/2k_B T} \quad 6$$

where E_G is the energy difference between the conduction band and the valence band. The temperature at which carrier promotions across the band gap are significant is usually much higher than room temperature, significant when $E_G \sim k_B T$. Typical band gaps of ~ 1 eV indicate that carrier promotions across the gap are significant at temperatures around 10,000 K. Promotions across the gap do occur at temperatures much lower than this, but they are outweighed by another effect: activation of carriers from the impurity level. For the temperature range of 10 K to 300 K examined in this text, activation of carriers from the impurity level is much more significant than activation of carriers from the valence band.

Promotions from the donor impurity level to the conduction band leave behind a hole in the impurity level. However, unlike the activation across the gap, this hole does not contribute to conduction [3, pg 137]. The temperature dependence for activation of carriers from the impurity level is given in Equation 7.

$$n(T) \propto e^{-E_D/k_B T} \quad 7$$

Since it is assumed that changes in mobility are outweighed by changes in carrier concentration, Equations 8 and 9 follow:

$$\ln(1/\rho) = A - \frac{E_G}{2k_B T} \quad 8$$

Equation 8 appears in literature [2, pg 87]. Equation 8 is applicable if the temperature is significantly high such that the Fermi level is approximately half way between the conduction and valence bands. This indicates that the impurity level has been depleted, and the change in carrier concentration arises from promotions across the gap. Conversely, when the impurity level has not been depleted and the Fermi level is half way between the impurity level and the conduction band,

$$\ln(1/\rho) = A - \frac{E_D}{k_B T} \quad 9$$

It can be seen from Equations 8 and 9 that the log of resistivity can be plotted against inverse temperature, and the slope of such a plot will yield an activation energy. This activation energy can be interpreted as either half of the band gap, or the energy difference between the valence band and the impurity level, as shown in Figure 2-2.

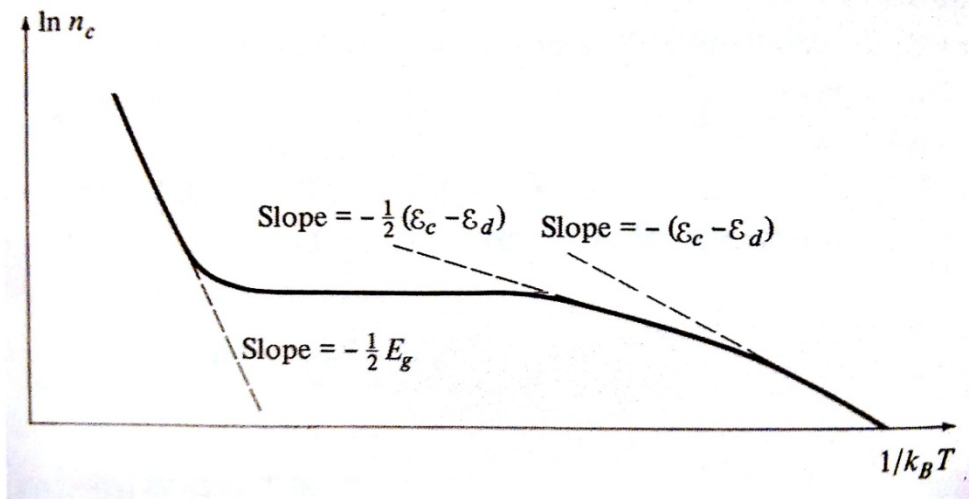


Figure 2-2: Carrier density temperature dependence of extrinsic semiconductor [5, pg 584]

Resistivity temperature dependence of metals

For metals, the conduction band at 0 K is partially filled, resulting in carriers that are free to move and contribute to conduction at temperatures marginally above 0 K. As temperature increases, the number of carriers in the conduction band does not vary significantly. The dominant property affecting the temperature dependence of resistivity is no longer carrier concentration, but rather the mobility of the carriers.

The mobility of carriers is affected by the frequency of collisions encountered as a carrier diffuses through a material. Higher temperatures increase vibrations within the material, and in turn increase collisions. The increased frequency of carrier collisions reduces the mean free path that each carrier travels between collisions, which in turn increases the resistivity of the material. Higher temperatures increase resistivity for metals and degenerate semiconductors. The slope of the increase in resistivity per unit temperature is known as the temperature coefficient of resistance (TCR).

Seebeck Effect - Metals and Semiconductors

When a heat gradient is applied across a material, a voltage difference is created between the hot and cold ends of the material. This phenomenon is known as the Seebeck effect. The magnitude of the Seebeck effect, known as the Seebeck coefficient, is the voltage difference per temperature difference. Equation 10 defines the Seebeck coefficient.

$$S \equiv \frac{V_C - V_H}{T_H - T_C} \quad 10$$

The Seebeck phenomenon arises from the diffusion of charge carriers. When heat is applied to one end of a material, carriers diffuse from the hot end to the cold end. As the carriers diffuse, the increased concentration of carriers at the cold end of the material creates an electric field. This electric field creates a force in the opposite direction of the thermal carrier diffusion, slowing down diffusion. At equilibrium, the thermal diffusion process is balanced by the resulting electric field, and the net carrier diffusion from one end of the material to the other is zero. The sign of the Seebeck coefficient is often used to indicate the carrier type of the material. A positive sign indicates that holes are the majority carriers, while a negative sign indicates that electrons are the majority carriers.

The units of the Seebeck coefficient are similar to the units of entropy, differing in units only the charge of an electron. The Seebeck effect is regarded as having an intrinsic relationship with entropy. Since charge carriers dissipate heat from one end of a material to the other, the thermodynamic relationship $dQ = TdS$ (dS being infinitesimal entropy in this relationship) implies each carrier diffuses entropy as it diffuses heat. The Seebeck effect is commonly thought of as entropy flux per unit carrier.

For metals, the Seebeck coefficient is given by Equation 11 [12, pg 305].

$$S = \frac{\pi^2 k_B^2 T}{e\mu} \quad 11$$

where μ is the chemical potential of electrons. Since the chemical potential is nearly independent of temperature, it can be inferred from Equation 11 that the Seebeck coefficient for metals is linearly proportional to temperature.

The temperature dependence of the Seebeck coefficient for semiconductors is a more complicated analysis. A common relation found in literature [9] relates the Seebeck coefficient to the electrical conductivity, and is shown in Equation 12. In Equation 12, + is chosen for an n type material, and – is for a p type material.

$$S = \pm \frac{k}{e} (\ln \sigma - \ln \sigma_0) \quad 12$$

Since the log of conductivity is proportional to $1/T$ (Equations 8 and 9), Equation 12 implies that the Seebeck coefficient is also proportional to $1/T$. This relationship is experimentally verified for high temperatures, but in contradiction to low temperature experimental data [12, pg 307]. Additionally, a $1/T$ dependence at low temperature contradicts the concept that the Seebeck coefficient is entropy flux per unit carrier, since the third law of thermodynamics requires that the entropy of a crystal should approach zero at absolute zero.

Goldsmid-Sharp – Seebeck Coefficient Analysis

An alternative explanation for why the Seebeck coefficient approaches zero at 0 K can be seen by considering the Seebeck coefficient as weighted by the conductivity of holes and electrons, as shown in Equation 13.

$$S = \frac{S_n \sigma_n + S_p \sigma_p}{\sigma_n + \sigma_p} \quad 13$$

From this weighted average one can see how the Seebeck coefficient at 0 K must approach zero. At 0 K for a semiconductor, $\sigma_n = \sigma_p$. Assuming $S_n = S_p$, the Seebeck effect of the n carriers will cancel with the Seebeck effect of the p carriers, resulting in a net Seebeck coefficient of zero. This is in agreement with the thermodynamic requirement that the Seebeck coefficient must approach zero at 0 K. Other texts [13] more rigorously show that viewing the Seebeck coefficient as weighted by the conductivities must imply that $S(T=0) = 0$.

Further analysis of Equation 13 leads to another conclusion: the band gap of a semiconductor can be estimated from temperature dependent Seebeck measurements [13]. The Goldsmid-Sharp band gap estimation, shown in Equation 14, shows the estimated band gap based on the maximum Seebeck coefficient S_{max} and the temperature T_{max} at which S_{max} occurs.

$$E_G = 2eT_{max} S_{max} \quad 14$$

The accuracy of the Goldsmid-Sharp band gap approximation is based on the assumption that the majority and minority carriers have the same mobility and effective mass. In the case of unequal mobilities of effective masses, the Goldsmid-Sharp band gap approximation has the error shown in Figure 2-3, where A is defined in Equation 15.

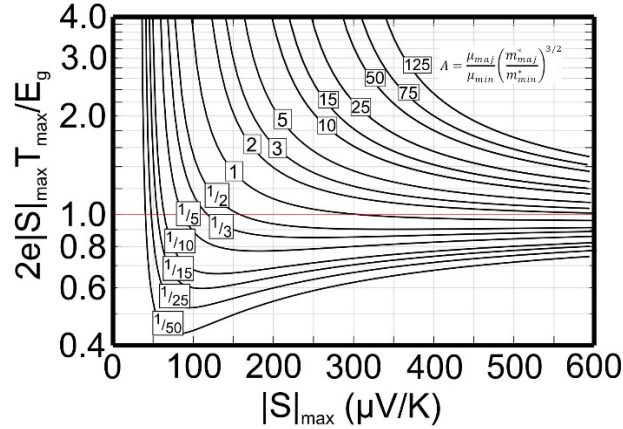


Figure 2-3: Error of Goldsmid-Sharp band gap approximation as a function of mobility and effective mass ratio of charge carriers.¹

$$A = \frac{\mu_{maj}}{\mu_{min}} \left(\frac{m_{maj}^*}{m_{min}^*} \right)^{3/2} \quad 15$$

Seebeck Coefficient Temperature Dependence - Summary

The Seebeck coefficient increases linearly with temperature for metals and degenerate semiconductors, as described by Equation 11. However, for semiconductors, the Seebeck coefficient depends on many variables and is not always accurately described by one equation. Semiconductors are often regarded as having a Seebeck coefficient that is inversely proportional to temperature. However, at low temperatures this violates the principles of thermodynamics. A general rule of thumb for the temperature dependence of the Seebeck coefficient for semiconductors is as follows: the Seebeck coefficient increases linearly with temperature until a certain temperature, and then decreases with temperature with a $1/T$ dependence. This rule of thumb is experimentally verified.

Jonker Plots – Thermopower and Resistivity comparison

Equation 12 compares the Seebeck coefficient to the electrical conductivity. It is common to plot the Seebeck coefficient versus the log of the conductivity. Such a plot is called a Jonker plot. By Equation 12, a slope of $\pm k/e$ is expected for such a plot. Observing this slope confirms that the material behaves as a typical semiconductor in a high temperature regime, with both S and $\log(\rho)$ proportional to $1/T$. The k/e slope is not observed for a degenerate semiconductor, since neither S nor $\log(\rho)$ is proportional to $1/T$ in the case of degeneracy. This slope will also not be observed for low temperatures, since S is not proportional to $1/T$ below a certain temperature.

¹ Figure referenced from: <http://thermoelectrics.matsci.northwestern.edu/thermoelectrics/index.html>
 Accessed 5/5/2015

For semiconductors in a high temperature regime, Equation 12 provides a method for estimating a maximum PF. The PF, written in terms of Equation 12 for a p type semiconductor, is shown below in Equation 16.

$$PF = S^2 \sigma = \left(\frac{k}{e}\right)^2 (\ln \sigma - \ln \sigma_0)^2 \sigma \quad 16$$

$$\frac{\partial(PF)}{\partial(\ln \sigma)} = \left(\frac{k}{e}\right)^2 e^{\ln \sigma} (\ln \sigma - \ln \sigma_0)(\ln \sigma - \ln \sigma_0 + 2) \quad 17$$

From Equation 17, it can be seen that the PF has extreme points at $\ln \sigma = \ln \sigma_0$ and $\ln \sigma = \ln \sigma_0 - 2$. Plugging these values into Equation 16 shows that $\ln \sigma = \ln \sigma_0$ corresponds to yields $PF=0$, and $\ln \sigma = \ln \sigma_0 - 2$ corresponds to a maximum. σ_0 can be extrapolated as the x intercept of a graph of S vs $\ln \sigma$. A qualitative Jonker Plot is shown in Figure 2-4. If the mobility is known, σ_0 can be inferred from a Jonker plot. The knowledge of σ_0 further allows the Density of States (DOS) to be calculated, given the relationship between σ_0 and the DOS as shown in Equation 18.

$$\sigma_0 = Ne\mu e^A \quad 18$$

N is the valence band DOS for a p type semiconductor, or the conduction band DOS or an n type semiconductor. A is a transport constant depending on the scattering parameters of the sample, usually $0 < A < 4$. If the mean free path of electrons is independent of the energy of the electrons, $A = 2$. If the mean free path of the electrons is proportional to the energy of the electrons, $A = 3$ [12, pg 306].

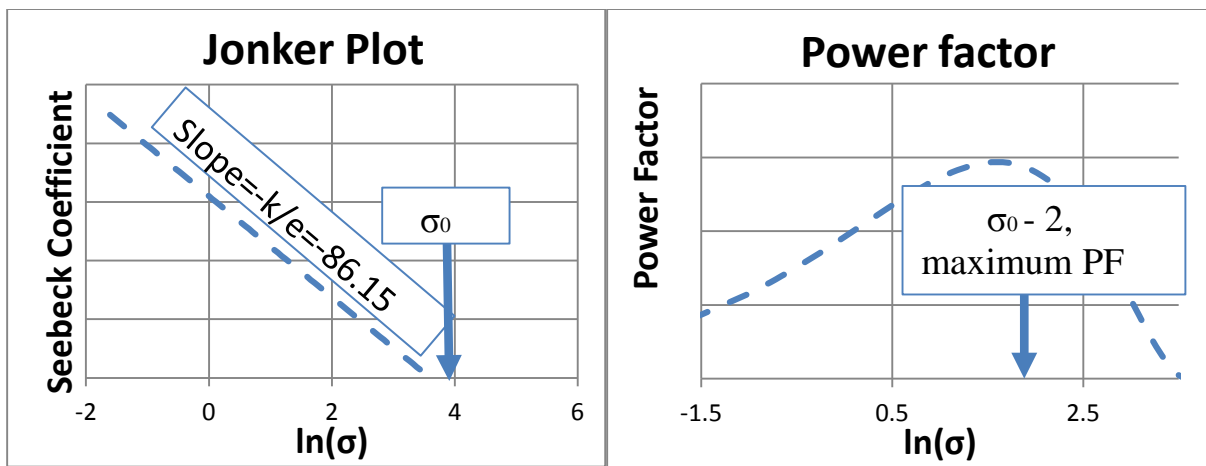


Figure 2-4: Qualitative power Jonker plot and power factor curve for non-degenerate semiconductors.

3. Materials

p Type and *n* Type Doping

A material is classified as either *p* type or *n* type to indicate the type of carrier. For an *n* type material, electrons are the dominant charge carrier in the material. For a *p* type material, an electron vacancy, referred to as a hole, is the dominant charge carrier. Impurities introduced into a semiconductor, a process known as doping, can change the semiconductor into a *p* type or *n* type material.

p type and *n* type materials can be created by replacing a small percentage atoms in the compound with a different element. Removing an atom and replacing it with an element with one more electron in its valence shell will bring an extra electron into the lattice. This extra electron will find a stable energy state just below the conduction band, known as the impurity level. Removing an element and replacing it with an element with one less electron in its valence shell will create a hole. The presence of holes in the lattice will create an impurity level in the band structure just above the valence band. Thus, doping a material by replacing a target element with an element to the *left* of it on the periodic table will create a *p* type material. Doping a material by replacing a target element with an element to the *right* of it on the periodic table will create an *n* type material.

p type and *n* type materials can also be created by creating vacancies in the material, a process known as doping with vacancies. Removing cations versus removing anions will have different effects on the material. Since cations donate their valence electrons to a bond, the removal of the cation element along with its donated valence electrons creates holes in the material. Similarly, since anion usually take electrons in a bond, the removal of an anion element will leave behind the electrons that it would have bonded with. Hence, doping with cation vacancies tends to create *p* type materials while doping with anion vacancies tends to create *n* type materials.

$\text{Cu}_3\text{Sb}_{1-y}\text{M}_y\text{S}_4$ ($\text{M}=\text{Sn}, \text{Ge}$)

Copper sulfide materials have been a recent area of active research, showing possible potential as a thermoelectric material [14]. The earth abundance of sulfur, combined with its low toxicity, makes it a desirable candidate for widespread production as a thermoelectric material if its figure of merit ZT can be optimized to a reasonable value. Cu_3SbS_4 shows promise as a thermoelectric material, with a high room temperature Seebeck coefficient, $S \approx 900 \mu\text{V}/\text{K}$. The direct band gap of Cu_3SbS_4 has been reported in literature as $\sim 0.9 \text{ eV}$ [14], and the measured band gap of Cu_3SbS_4 examined in this paper is $\sim 0.85 \text{ eV}$.

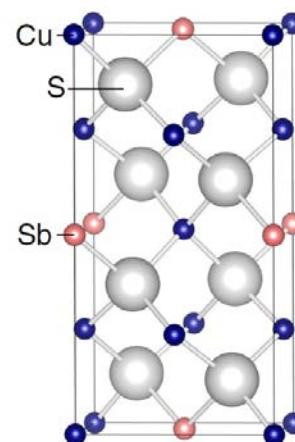


Figure 3-1: Crystal Structure of Cu_3SbS_4 ³

² Dr. Robert Kokenyesi, private conversation

³ Figure obtained from “Effect of Sn-Substitution on Thermoelectric Properties of Copper-Based Sulfide, Famatinitite Cu_3SbS_4 ” [14]

This paper focusses on electrical transport measurements of bulk $\text{Cu}_{3-x}(\text{Sb}_{1-y}\text{M}_y)\text{S}_4$ ($\text{M}=\text{Sn,Ge}$), for $x = 3\%$ and $y = 1\%, 5\%$.

Indium Tin Oxide (ITO)

ITO is a widely used material known for its low electrical resistivity and optical transparency. Due to these attractive properties, ITO is commonly used in production of electronic devices and is well characterized in literature. The well-known properties of ITO make it an ideal candidate for calibrating and testing new experimental setups, as is done in this paper. The physical properties of ITO depend on varying proportions of SnO_2 and In_2O_3 . ITO is usually fabricated in such a way as to produce a highly conductive material that behaves as a degenerate semiconductor. Optimal proportions for high conductivity have been found to be 5% SnO_2 by weight and 95% In_2O_3 by weight [15]. The resistivity of ITO can be on the order of $200 \mu\Omega \text{ cm}$, with mobilities ranging from 15 to 40 $\text{cm}^2/\text{V}\cdot\text{s}$ [15].

Bismuth Telluride

Bismuth telluride (Bi_2Te_3) is a common benchmark as a thermoelectric material, with a high figure of merit ZT and power factor PF . Bismuth telluride can be fabricated as a p type material with $ZT \sim 1$ and $PF \sim 4.8 \times 10^{-3} \text{ W/K}^2\text{m}$ [11]. Bismuth telluride is a moderately rare material. It possesses a narrow band gap of 0.2 eV, and has been a longstanding subject of research due to its standing as a good thermoelectric material. Bi_2Te_3 will be the benchmark to which Cu_3SbS_4 is compared in this paper.

4. Methods

The following sections describe the experimental setup used to measure electrical resistivity and thermopower for temperatures between 10 K and 300 K. This experimental setup has been recently redesigned by the author to allow for simultaneous measurement of these two properties. Because of this recent re-design, the methodology will be examined in depth. A COMSOL Multiphysics model of the system is also examined at the end of this section to analyze the accuracy of the system.

Cryogenic Setup and Methodology

A Helium cryocooler and a Lakeshore DRC-91AC temperature controller are used to achieve and maintain temperatures as low as 10 K. The cryostat setup is shown in Figure 4-1. The helium cryocooler operates using the Gifford-McMahon refrigeration cycle, with 99.999% pure helium used as the refrigerant. In the Gifford-McMahon cycle, the expansion of helium gas acts as the driving cooling power to draw heat out of the system. The helium cryocooler cold head consistently achieves temperatures as low as 10 K. If care is taken to tightly wrap all wires close to the inner core of the cold head, even the top of the experiment is consistently cooled to 10 K as measured by a Type K thermocouple.

A vacuum is drawn inside the cryostat chamber to insulate the chamber. Cooling can begin once vacuum pressure has reached of 5×10^{-5} torr or lower. With a vacuum drawn, the primary means of heat entering the experimental setup is through radiation. The cryostat is designed with two metal shields: an inner shield and an outer shield. The inner shield blocks radiation from the room temperature outer shield. This minimizes the amount of radiation reaching the experimental setup.

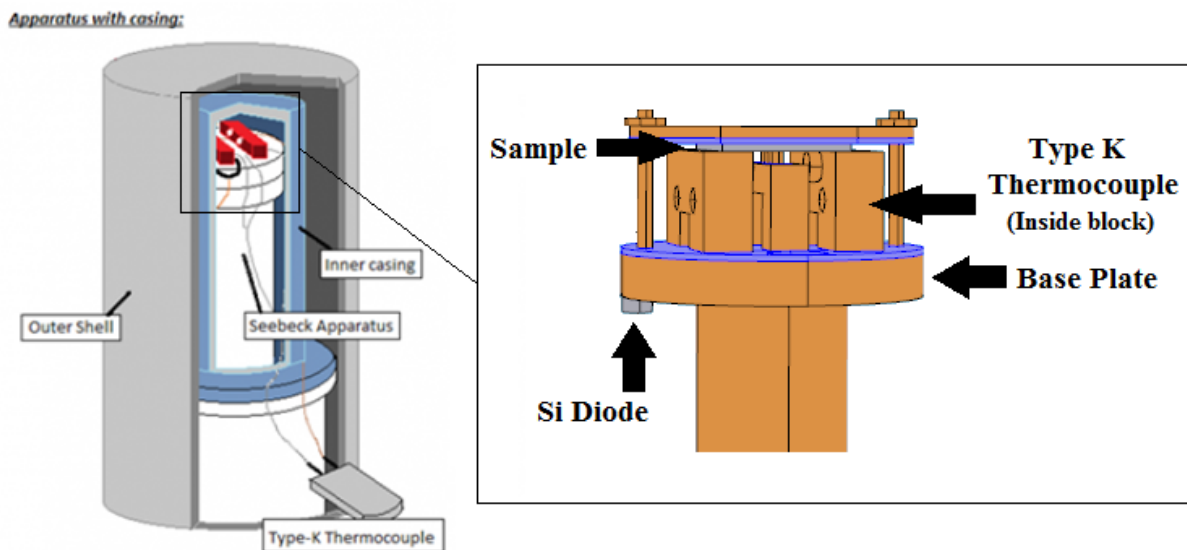


Figure 4-1: Cold head apparatus with experimental setup shielded by the inner casing⁴. Location of Si Diode and Type K thermocouple shown on the right.

⁴ Figure on left hand side created by Rachel Waite.

The temperature inside the cryostat is measured at the baseplate with a silicon diode, as well as closer to the sample with a Type K thermocouple. During the cooling stage, the baseplate cools much faster than the top because it is closer to the cold head. During warming, the base and top are much closer to thermal equilibrium with each other. Since thermal non-equilibrium affects the accuracy of the experiment, data collected during the warming stage are preferred over data collected during the cooling stage.

Resistivity data are collected during cooling and warming, but the cooling data are usually discarded due to the thermal non-equilibrium. Thermopower data are collected only during warming, since collecting thermopower data requires operating a heater, which would hinder the cooling process. The cryostat is chilled until the temperature recorded by the Type K thermocouple either matches the temperature of the silicon diode, or plateaus. The temperature recorded by the Type K thermocouple may plateau at 20 K or higher if wires are not tightly wrapped around the cold head. The silicon diode consistently measures temperatures as low as 10 K at the base. The Type K thermocouple can consistently achieve 10 K as well if wires are tightly wrapped around the cold head.

Once a minimum temperature is attained, the system is gradually warmed while Seebeck coefficient data is collected. A Lakeshore 320 temperature controller⁵ is used to achieve temperature set points in 10 K increments. After incrementing the temperature set point, it usually takes ~30 minutes for the system to achieve thermal equilibrium. At this point, the Seebeck coefficient measurement is performed and then this process is repeated.

At about 150 K⁶, the cryostat warms slowly enough to simply turn off the cryopump and collect thermopower data while the cryostat warms. If thermopower data is not required, the cryopump can be turned off sooner than 150 K. The resistivity experiment is performed quickly enough to not require holding the temperature constant. This process is shown visually as a flow chart in Figure 4-2.

⁵ The author has found it preferential to use the LS320 temperature controller rather than the LS91C controller. The LS320 senses temperature from the Si diode, farther away from the sample. Despite being farther away from the sample, the Si diode is closer to the heater used to warm the cryostat. Using the LS91C controller requires a longer time to achieve equilibrium because it senses temperature with the Type K sensor, located farther away from the cryostat heater.

⁶ The author is in the process of determining the optimal temperature at which to transition from manually controlling the temperature to allowing the cryostat to warm. Each iteration of setting a temperature set point, waiting for equilibrium, and taking data takes about 40 minutes. Doing this process from 10 K to 150 K takes about ten hours.

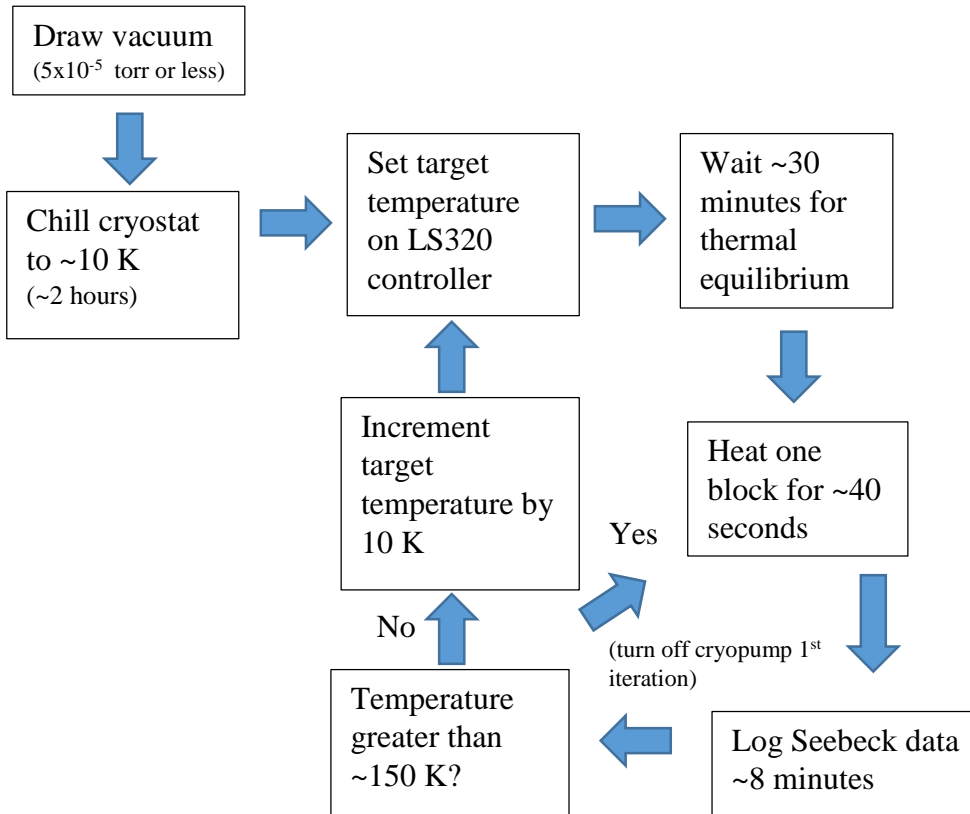


Figure 4-2: Flow diagram for performing temperature dependent thermopower measurements. Times shown can be increased to increase quality of measurements, or decreased to hasten the experiment. Not shown: resistivity data is logged simultaneous to this process.

The process of collecting thermopower data requires the system to be in thermal equilibrium prior to performing measurements. For low temperatures, thermal heat transfer takes a longer time to achieve thermal equilibrium. Each thermopower measurement requires approximately 30 minutes to thermally stabilize prior to beginning the measurement, ~30 to ~60 seconds to heat one block, and then about 10 minutes of data collection while the hot block cools. This process has been automated with LabView code.⁷ The optimal lengths of time for heating and data collection vary from sample to sample, and depend on the thermal conductivity and specific heat of the sample.

Inline Four Probe Resistivity Measurement

Resistivity is measured with an inline four-probe contact method. Four probes are needed rather than two because each probe creates a contact resistance between the probe and sample. This contact resistance is not negligible and introduces an error into a two-probe measurement, where it is impossible to deduce what percentage of the measured resistance is from the sample, and what percentage is from the contact resistance.

⁷ See version 10.1 of the Seebeck LabView program located in the LabView folder on the T drive.

Using four probes rather than two allows for the effect of the contact resistance to be minimized. The four-probe method uses four, equidistant probes to make electrical contact with a material. The outer two probes send a current through the material while the inner two probes measure the potential. The inner probes create a small current to measure the potential. A circuit diagram of the four-probe method is shown in Figure 4-3.

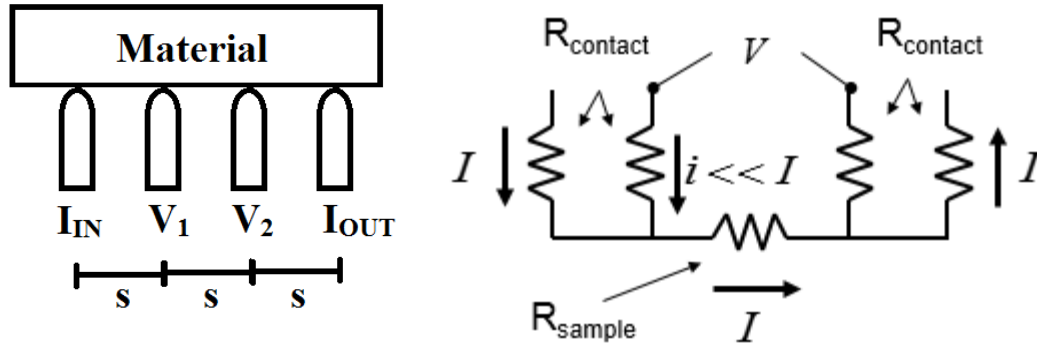


Figure 4-3: Four probe contact pins and material (left) and equivalent circuit diagram (right)⁸

The voltage measured by the inner probes is shown in Equation 19. Because the inner probes represent a large impedance voltmeter and create a very small current, the effect of the contact resistance is negligible. The resistance measured by the inner probes is approximated by Equation 20.

$$V = IR_{sample} + i(2R_{contact} + R_{sample}) \quad 19$$

$$V \approx IR_{sample} \quad i \ll I \quad 20$$

Seebeck Coefficient Measurement

To measure the Seebeck coefficient, two electrically isolated copper blocks are laid on top of the cold head in the cryostat. Current is run through a resistor that is in thermal contact with one of these blocks, dissipating heat and warming this block. The block warmed by this resistance heater is referred to as the hot block, while the block not warmed is referred to as the cold block. The setup is shown in Figure 4-4.

⁸ 4 probe circuit diagram Figure created by Daniel Harada, 2010-11-8 presentation

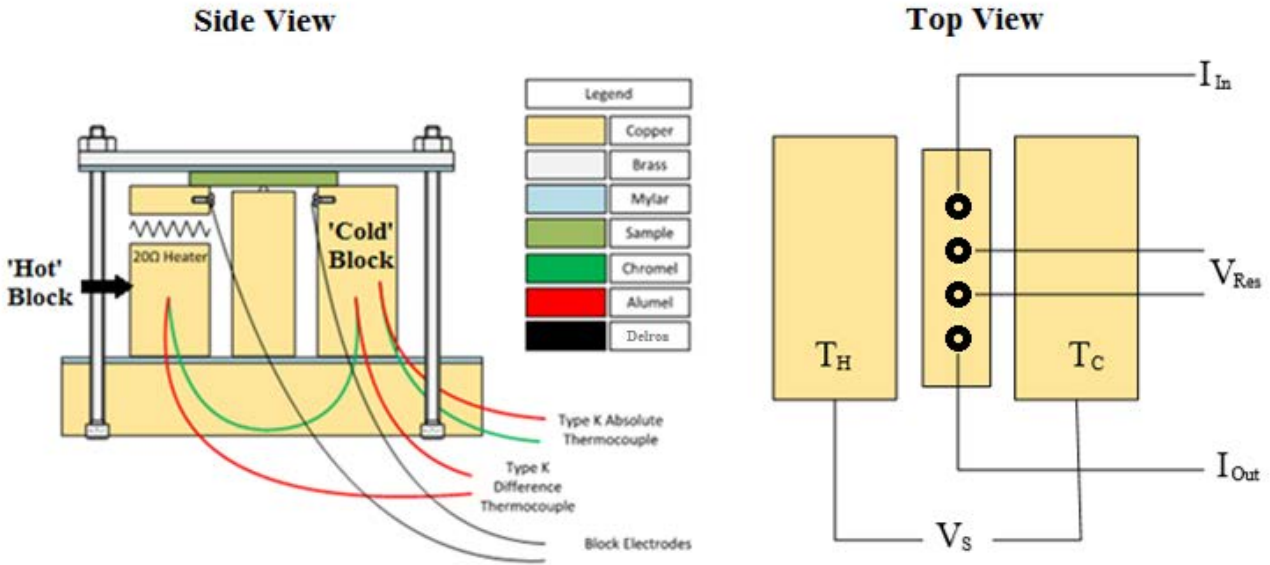


Figure 4-4: Experimental setup. Side view (left) and top down view (right)

Mylar is used as an electrical insulator to insulate the blocks from the base of the experiment. A sample is laid across the copper blocks, in thermal and electrical contact with each block. The temperature difference between the blocks generates a temperature difference of about 0 - 2 K across the material, in turn creating a voltage difference across the material and between the blocks. This voltage difference is proportional to the Seebeck coefficient of the material. The absolute temperature is measured with a Type K thermocouple in contact with the cold block, and the temperature difference between the blocks is measured using another thermocouple, referred to as the difference thermocouple. The potential difference between the blocks is measured with wire leads in contact with each block. The potential difference between the blocks is plotted against the temperature difference, and the slope yields the Seebeck coefficient of the material. A dataset is shown in Figure 4-5. This process is repeated while the temperature is held at different target set points.

The difference thermocouple, shown in the left hand side of Figure 4-5, consists of two chromel/alumel junctions that are in thermal contact with (but electrically insulated from) each copper block. The temperature difference between the two blocks creates a voltage difference between the two alumel leads. This voltage difference is converted to a temperature difference using a known voltage to temperature calibration that can be found in a thermocouple handbook. At room temperature, this calibration is 40 $\mu\text{V/K}$ for a Type K thermocouple. At lower temperatures this conversion between voltage and temperature becomes smaller in magnitude.

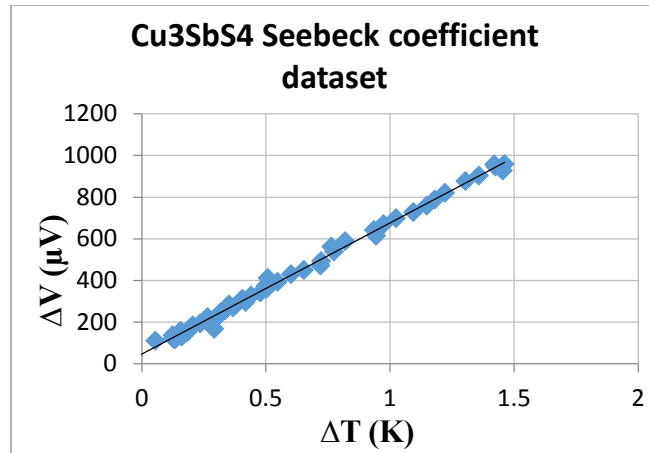
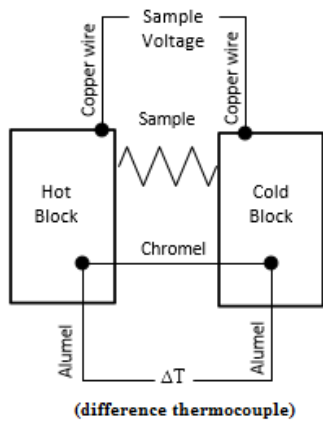


Figure 4-5: Schematic of measuring apparatus (left). Dataset for Cu₃SbS₄ (right)

Simultaneous resistivity & thermopower measurement

Previous configurations of the experimental setup allowed either resistivity or thermopower to be measured at one time. The previous system, shown in Figure 4-6 (left), required the sample to be placed face down to measure the Seebeck coefficient or face up to measure the resistivity. The current physical setup, designed by the author, measures both the Seebeck coefficient and the resistivity with the sample laid face down. Since each dataset of temperature dependent measurements requires several hours of overhead associated with drawing a vacuum and chilling the cryostat, this simultaneous measurement saves a significant amount of time. The old and current setups are shown in Figure 4-6.

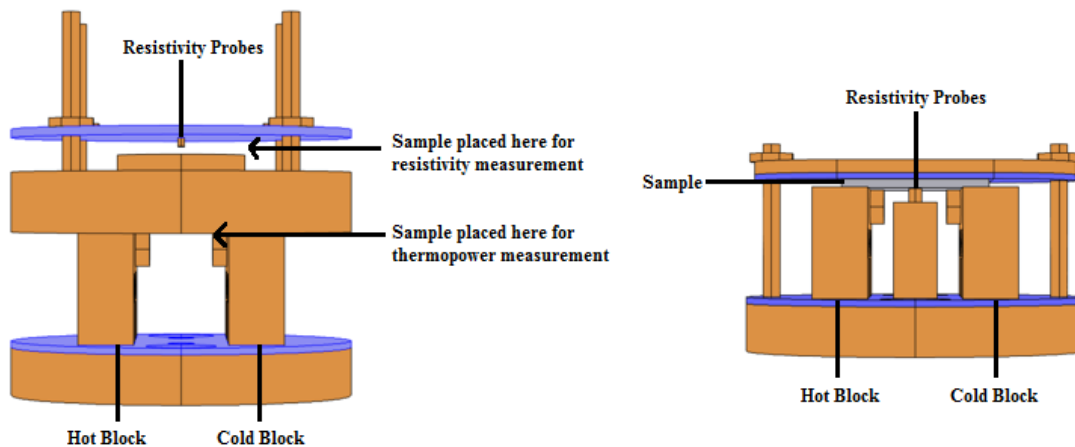


Figure 4-6: Previous (left) and current (right) experimental setup

Since the current setup’s four resistivity probes are parallel to the copper blocks and perpendicular to the thermal gradient, (Figure 4-4 and Figure 4-6, right), the thermal gradient does not interfere with the resistivity measurement. The resistivity probes are along a line of constant temperature along the sample. As a precaution, any thermal gradient in the system is filtered out by taking the resistivity measurement twice, with the current direction reversed in the second measurement. The Keithley 2400 source/meter used to measure resistivity is set to automatically do this. The temperature corresponding to the measured resistivity is taken to be the temperature measured by the Type K thermocouple, plus half of the temperature difference between the two blocks.

COMSOL Modeling

To examine the heat transfer properties of the experiment, a model was constructed⁹ of the system using COMSOL Multiphysics software with the Heat Transfer in Solids package. The Heat Transfer in Solids package solves the heat transfer equation shown in Equation 21 using the finite element method.

$$\rho C_p \frac{\partial T}{\partial t} - \nabla \cdot (K \nabla T) = Q \quad 21$$

The heating process of the thermopower experiment was simulated in the model. A heat source dissipates ¼ watt of power onto one of the copper blocks for 45 seconds. To simulate the cold head actively chilling the experiment, the base of the experiment (bottom of Figure 4-7) is kept at a constant temperature within the simulation. This simulation is repeated using the cryogenic properties of the experimental materials at 20 K, 50 K, and 300 K shown in Appendix 1, and the results are shown in Figure 4-8.

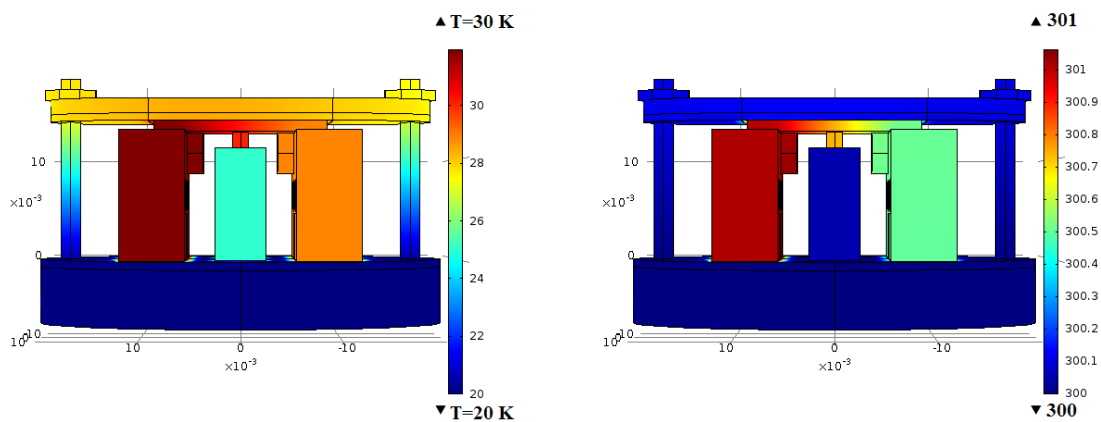


Figure 4-7: COMSOL heat transfer model of experimental setup at 20 K (left) and 300 K (right). See Appendix 1 for summary of cryogenic material properties and assumptions made in the COMSOL model.

⁹ The COMSOL model is located on the T drive in the following directory:
T:\Physics\Tate Group\Share\Mutch, 2014 – current\COMSOL Files\Cyrogenic_Transport_Apparatus.mph

A linear temperature gradient across the sample is observed in the COMSOL model, between 0.5 K and 1.3 K. Interesting trends are observed between the high temperature and room temperature simulations, which result from the different cryogenic material properties of the sample used in the simulation (silicon) and the copper blocks. A summary of the cryogenic properties used in the simulation is given in Appendix 1.

At low temperatures, thirty seconds of heating in the simulation results in a lower temperature difference (ΔT) between the blocks compared to high temperatures. It has been experimentally observed that the ΔT generated at low temperatures can be different from the ΔT generated at high temperatures. The ΔT can be higher or lower at low temperatures compared to room temperature, and depends on the sample's material properties. A possible concern is that the thermal conductivity of the sample in contact with the blocks is very high. If a sample's thermal conductivity is too high, heat from the hot block will be quickly conducted to the cold block and no temperature difference is generated. In the simulation, at 50 K and the sample's thermal conductivity set to 1000 W/m/K, the cold copper block is warmed a few tenths of a kelvin. The cold copper block is warmed by roughly twice this amount for room temperatures.

Figure 4-8 shows the COMSOL simulation heating response of the apparatus for different samples at different temperatures, as a function of the thermal conductivity of the sample. It can be seen from Figure 4-8 that as the sample's thermal conductivity approaches 1000 W/m/K, the heat from the hot block is conducted to the cold block, and the apparatus struggles to create a temperature difference between the blocks. It should be kept in mind that this apparatus may not be effective for samples with extremely high thermal conductivity.

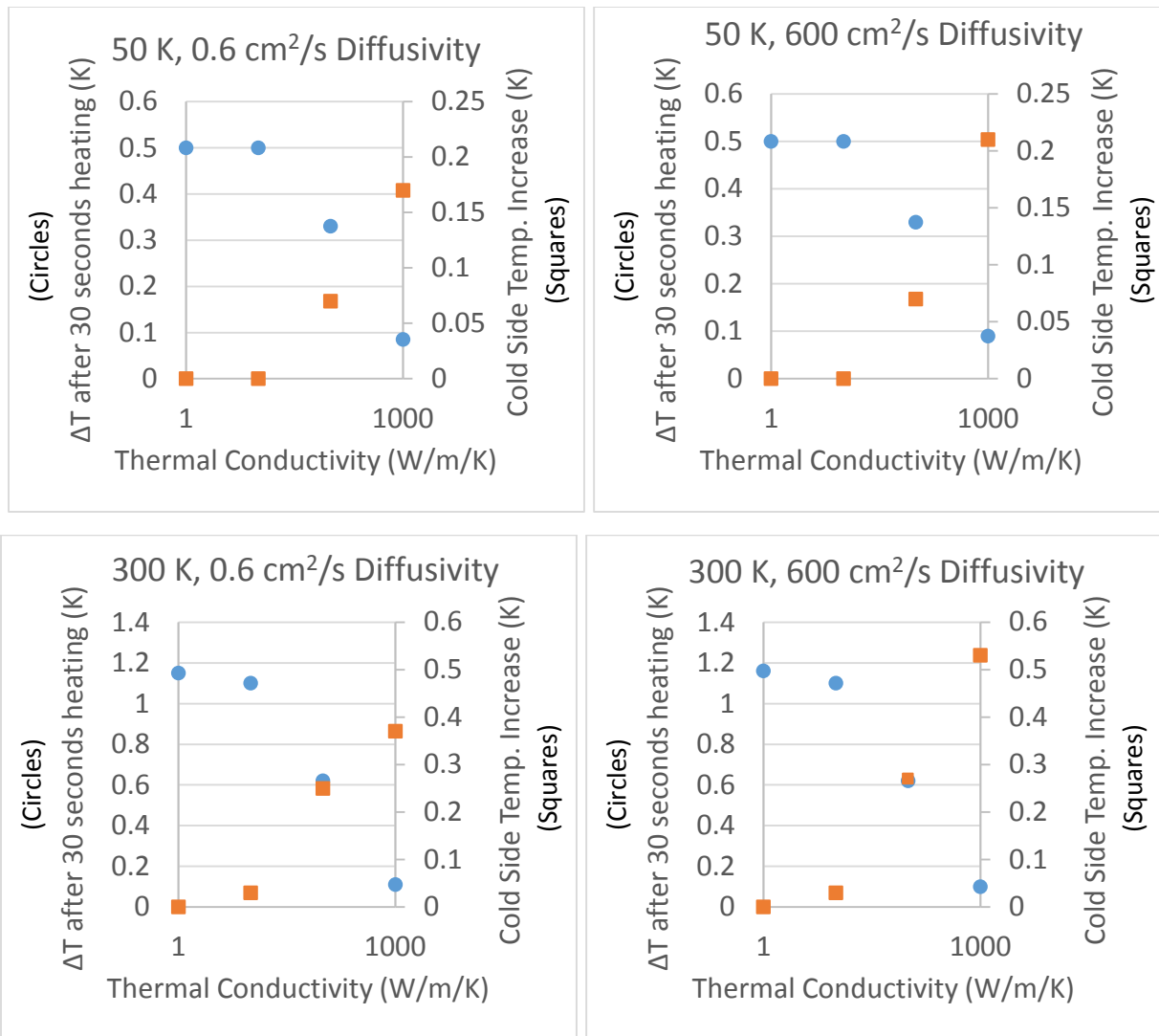


Figure 4-8: Heating response of the experimental apparatus, simulated with COMSOL Multiphysics software. The density of silicon (2330 kg/m^3) was assumed to calculate specific heat corresponding to the labeled thermal diffusivity value.

4. Results

Indium Tin Oxide

The resistivity and Seebeck coefficient of an ITO thin film¹⁰ were simultaneously measured using the apparatus described in the Methods section. Data were taken from 10 K to 300 K. Resistivity was also measured using a Van Der Pauw configuration from 300 K to 450 K. The results are shown in Figure 4-1 (left). Figure 4-1 (right) also displays transport measurements of a different ITO sample for comparison. The trends of the resistivity and Seebeck coefficient between these two samples agree with each other, with slight differences in the magnitude of these properties arising from sample to sample variability.

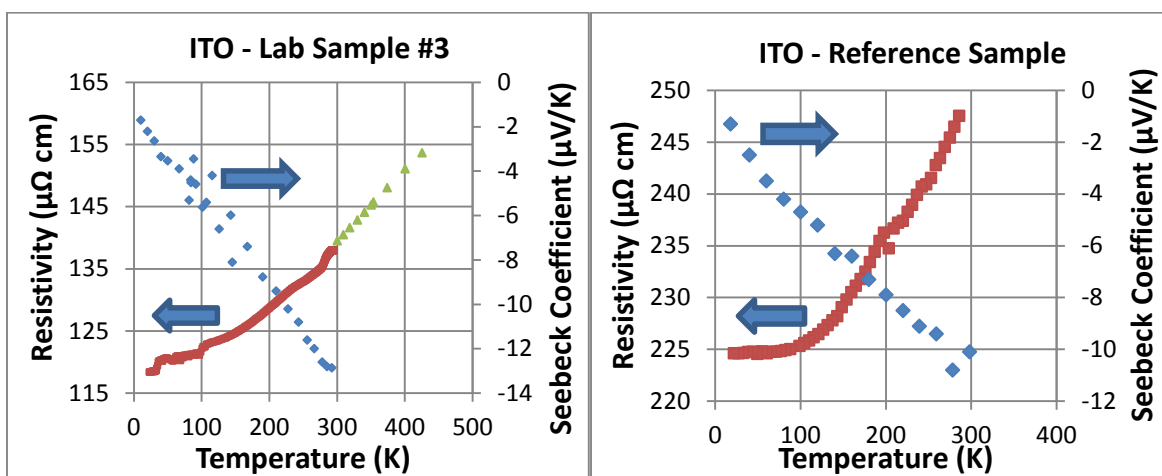


Figure 4-1: Transport measurements for two different samples of thin-film ITO, fabricated under different conditions.

The ITO results shown in Figure 4-1 agree with results for a degenerate semiconductor that behaves as a metal. The magnitude of the negative Seebeck coefficient and the resistivity both linearly increase with temperature above 100 K. Below 100 K, the resistivity approaches a constant value.

Cu₃SbS₄

Transport measurements for bulk Cu_{3-x}(Sb_{1-y}M_y)S₄ (M=Sn,Ge) samples were made, for $x = 0$, $x = 3\%$, $y = 1\%$, $y = 5\%$. Figure 4-2 shows the resistivity and thermopower results. These results are analyzed with Jonker analysis in Figure 4-3. The activation energies of $x = 0$, $x = 3\%$, and the 1% Sn sample are analyzed Figure 4-4. A summary of results is given at the end of this section in

100 K	Seebeck Coefficient (μV/K)	Resistivity (Ω cm)	Power Factor (W/K ² m)	Activation Energy (meV)
$x = 0$	102	307.1	0.0034	20
$x = 3\%$	449	90	0.22	46
M=Sn, $y = 1\%$	55	0.099	3.10	0.1 (20 K)

¹⁰ Lab name: ITO Sample #3, ~160 nm thickness

M=Sn, y = 5%	28	0.018	4.34	-
M=Ge, y = 5%	36	0.0053	25	-

Table 4-1.

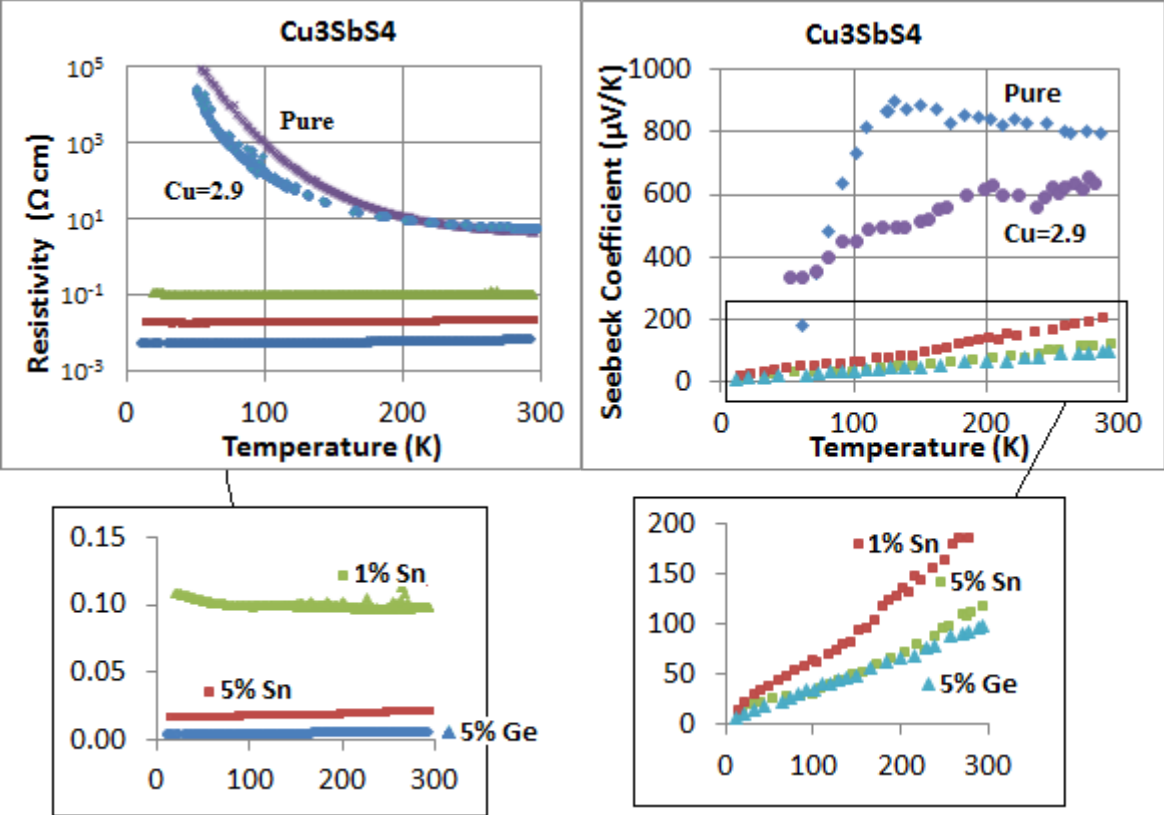


Figure 4-2: Bulk Cu_3SbS_4 resistivity measurements (left) and thermopower measurements (right)

The resistivity and Seebeck coefficient measurements are shown above in Figure 4-2. The resistivity of the pure sample increases exponentially with decreasing temperature. Doping with copper vacancies ($x = 3\%$) slightly decreases the resistivity, but the resistivity still increases exponentially with decreasing temperature. Doping the Sb sites with Sn and Ge dramatically lowers the resistivity and behavior of the temperature dependence. With 1% Sn doping, the resistivity slightly increases with decreasing temperature. With 5% Sn and 5% Ge doping, the resistivity linearly decreases with decreasing temperature, indicating a degenerate, metallic-like material.

The Seebeck coefficient of pure Cu_3SbS_4 has a maximum of $900 \mu\text{V/K}$ at $T=130 \text{ K}$. Above this temperature, the Seebeck coefficient decreases with increasing temperature, but is not proportional to $1/T$. Doping with copper vacancies decreases the magnitude of the Seebeck

coefficient, but the experimental noise of the Seebeck coefficient measurement prohibits a definitive statement to be made about the trend of this property. For the samples with Sn and Ge doping, the Seebeck coefficient is reduced by 75% or more and found to decrease linearly with decreasing temperature.

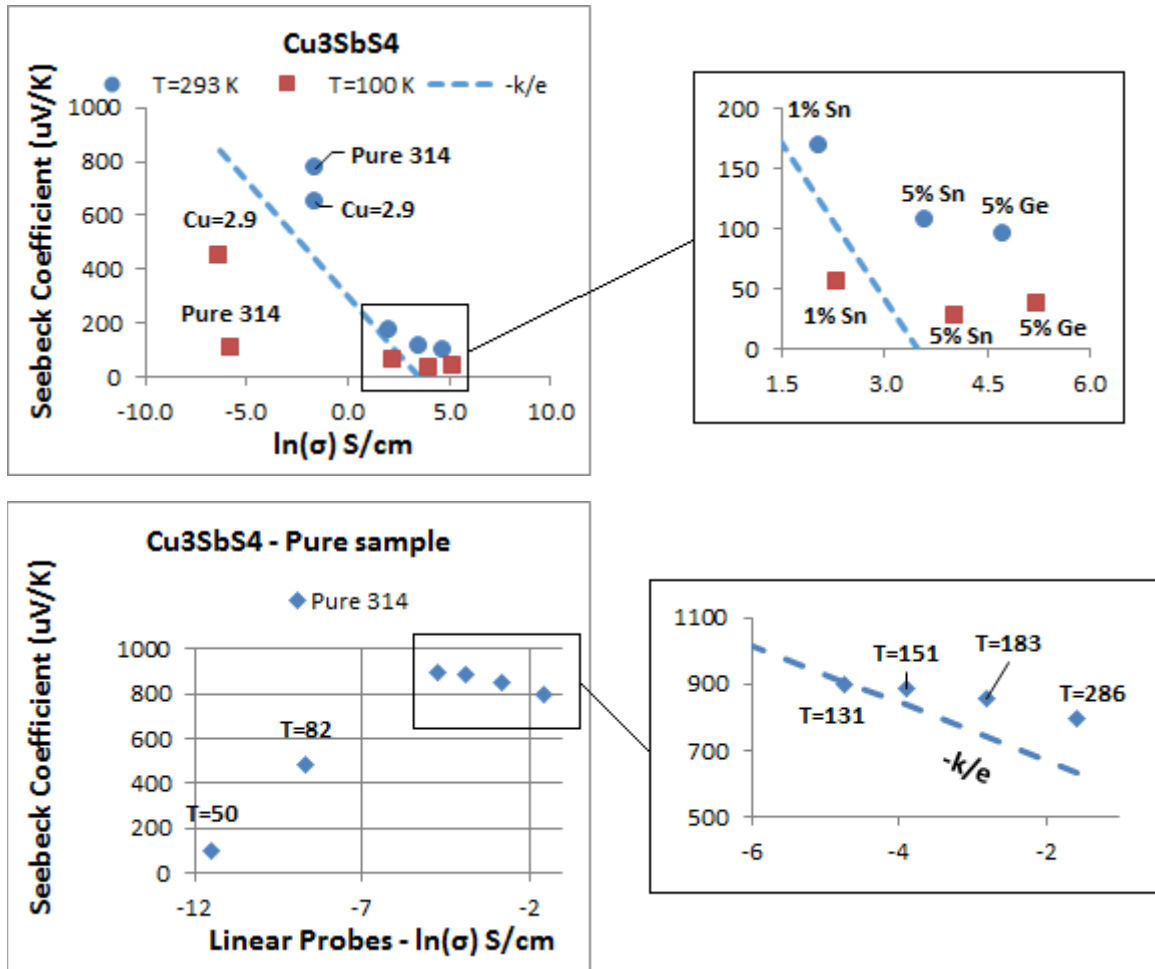


Figure 4-3: Cu_3SbS_4 Jonker analysis at room temperature (left) and 100 K (right). A line with a slope of $-k/e$ and an arbitrary intercept has been fitted in each graph

Jonker analysis of variants of Cu_3SbS_4 is shown in Figure 4-3. A theoretical slope of $-k/e$ has been placed (with an arbitrary intercept) to aid the eye to see the theoretical Jonker trend. It is seen that these samples do not adhere to this trend. The degenerate samples (doping with 1% and 5% Sn, and with 5% Ge) display a slope with a smaller magnitude to the k/e slope. The pure Cu_3SbS_4 sample also displays a slope smaller than k/e at temperatures between 130 K and 300 K, the temperature range during which the Seebeck coefficient decreases with temperature. For

temperatures from 10 K to 130 K, the pure sample and the sample with copper vacancies do not adhere to the Jonker trend.

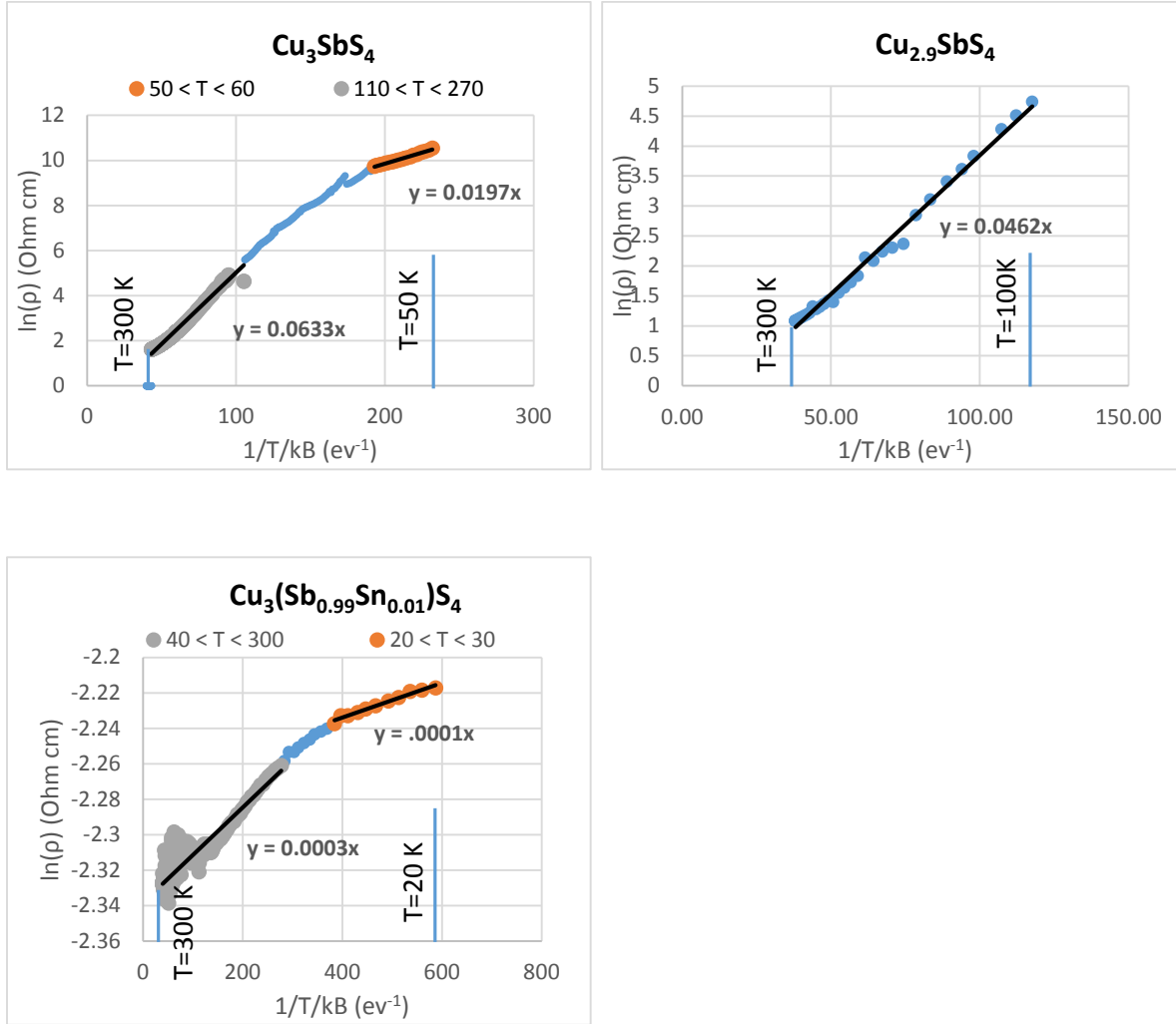


Figure 4-4: Activation energy analysis for Cu_3SbS_4 . Pure sample (upper left), Cu=2.9 (top right), and 1% Sn sample (bottom left).

Figure 4-4 shows activation energy analysis for pure Cu_3SbS_4 , doping with Cu vacancies, and doping with 1% Sn. The y axis is the natural log of the resistivity, and the x axis is inverse temperature divided by the Boltzmann constant, k_B . The slope of such a plot reveals the activation energy of the sample, as seen from the relation between resistivity ρ and the activation energy E_A shown in Equation 21.

$$\ln(1/\rho) \propto \frac{E_A}{k_B T}$$

For a temperature range between 10 K and 300 K, the activation energy E_A for a p type material is interpreted as the energy difference between the impurity level and the valence band, as shown in Equation 9 and Figure 2-2 in the Theory section.

Room Temperature	Seebeck Coefficient ($\mu\text{V/K}$)	Resistivity ($\Omega \text{ cm}$)	Power Factor ($\mu\text{W/K}^2\text{m}$)	Activation Energy (meV)
x = 0	771	4.8	12.4	63
x = 3%	650	4.6	9.1	46
M=Sn, y = 1%	169	0.13	22.2	0.3
M=Sn, y = 5%	107	0.027	42.3	-
M=Ge, y = 5%	96	0.0088	103.9	-

100 K	Seebeck Coefficient ($\mu\text{V/K}$)	Resistivity ($\Omega \text{ cm}$)	Power Factor ($\text{W/K}^2\text{m}$)	Activation Energy (meV)
x = 0	102	307.1	0.0034	20
x = 3%	449	90	0.22	46
M=Sn, y = 1%	55	0.099	3.10	0.1 (20 K)
M=Sn, y = 5%	28	0.018	4.34	-
M=Ge, y = 5%	36	0.0053	25	-

Table 4-1: Summary of electrical transport results for $\text{Cu}_{3-x}(\text{Sb}_{1-y}\text{M}_y)\text{S}_4$ (M=Sn,Ge) at room temperature and 100 K

6. Discussion

Of the variants of Cu_3SbS_4 examined, the sample doped with 5% Ge occupying the Sb site displayed the highest power factor. The 5% Ge sample measured $S=95 \mu\text{V/K}$ and $\rho=20 \text{ m}\Omega \text{ cm}$, for $PF=1.04 \times 10^{-4} \text{ W/K}^2\text{m}$. This PF is 2.2% of the benchmark PF of bismuth telluride, indicating a lack of promise as a thermoelectric material. This maximum power factor occurred at room temperature, $\sim 300 \text{ K}$. The temperature trends of the Seebeck coefficient (increasing with temperature) and the resistivity (slightly increasing with temperature) indicate that the PF will increase with higher temperatures. However, unless a dramatic change in these trends occurs, the PF will not be competitive, even at higher temperatures.

The resistivity of pure, bulk Cu_3SbS_4 behaved as semiconductors between 10 K and 300 K, with an increasing activation energy with increasing temperature. This increasing activation energy is at variance with the predicted trend seen in Figure 2-2, which predicts a decreasing activation energy with increasing temperature. In this temperature range, the Seebeck coefficient displayed a change in behavior, switching between increasing with temperature to decreasing with temperature at 130 K. It has been noted in some texts that the temperature at which the Seebeck coefficient transitions between two trends sometimes corresponds to a change in activation energy [12, pg 311]. The implications of this temperature at which S is maximum and the changing activation energy are uncertain.

Doping with Sn or Ge on the Sb sites creates additional holes, as does doping with copper vacancies. Doping with holes should produce a p type material, similar to the pure sample. All measured samples were p type materials, in agreement with this reasoning. The introduction of these additional carriers also increased conductivity, at the expense of decreasing the Seebeck coefficient.

1% doping with Sn reduces the room temperature Seebeck coefficient by $\sim 75\%$, and produces a constantly decreasing Seebeck coefficient with decreasing temperature. The 5% doping with Sn and Ge amplified the reduction in the magnitude of the Seebeck coefficient. Doping with 3% copper vacancies results in a less dramatic impact on the Seebeck coefficient, with a room temperature reduction of $\sim 20\%$ compared to the pure sample. The noise of the Seebeck coefficient measurement on the 3% vacancies sample prohibits a conclusion being made as to the temperature dependence of this sample. It is unsure if the temperature dependence is strictly linear, or if there is a temperature range at which the Seebeck coefficient is constant.

Jonker analysis does not offer insight when comparing samples of different doping amounts, since the doped samples do not display a $1/T$ dependence for the Seebeck coefficient. For the pure sample, Jonker analysis of the sample at temperatures higher than 130 K displays a slope with a smaller magnitude than the predicted k/e . This is because the Seebeck coefficient is not proportional to $1/T$. Although the Seebeck coefficient decreased with increasing temperature above 130 K, it decreased at a slower rate than $1/T$.

The measurement of a maximum Seebeck coefficient provides an opportunity to apply Goldsmid-Sharp analysis to predict the band gap of the sample. Using the measured data ($S_{\max} \sim 900 \mu\text{V/K}$, $T_{\max} \sim 130 \text{ K}$) and Goldsmid-Sharp methodology, a band gap of band gap of 0.23 eV is calculated. This does not agree with the measured band gap of 0.85 eV. This disagreement between Goldsmid-Sharp analysis and the measured band gap possibly implies unequal mobilities and effective masses between the majority and minority carriers. In future iterations of this experiment, it would be beneficial to measure the effective masses and mobilities of the majority and minority carriers. If these properties of the majority and minority carriers were found to be relatively equal, it would imply that the Goldsmid-Sharp analysis is inapplicable for this material.

7. Conclusion

A cryogenic electrical transport measurement apparatus was modified to measure both the Seebeck coefficient and resistivity simultaneously. A COMSOL Multiphysics software model was constructed to analyze the thermal transport properties of the apparatus. The COMSOL model showed that the apparatus was capable of generating a temperature difference across a sample for samples with a thermal conductivity less than $1000 \text{ Wm}^{-1}\text{K}^{-1}$. The magnitude of the temperature difference ranged from 0.1 K to 1.2 K after 30 seconds of heating, and was dependent on the thermal conductivity and diffusivity of the sample.

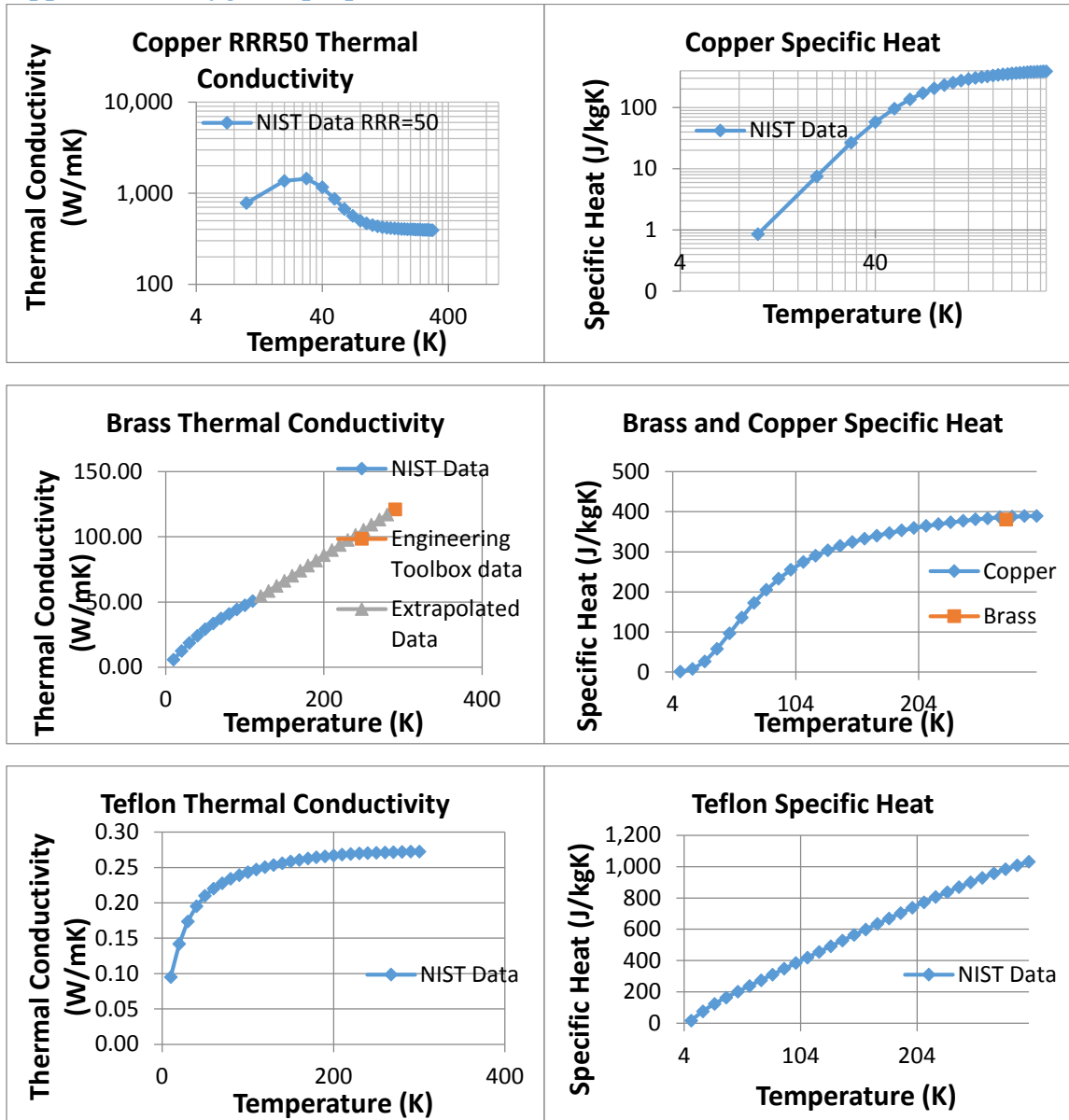
The resistivity and Seebeck coefficient of Cu_3SbS_4 and several doped variants were measured using this apparatus. The 5% Ge sample displayed the highest PF of $1.04 \times 10^{-4} \text{ W/K}^2\text{m}$. This value is 2.2% of the benchmark PF of bismuth telluride, indicating these samples are not promising as thermoelectric materials. These samples do not fit a Jonker analysis model, since the Seebeck coefficient is not proportional to $1/T$. Despite Jonker analysis not providing accurate predictions for these samples, Jonker analysis should be used in the analysis of future samples using the data generated by this experimental setup. Jonker analysis can provide useful insight into the intrinsic conductivity and DOS for samples with a $1/T$ dependence for both the resistivity and Seebeck coefficient.

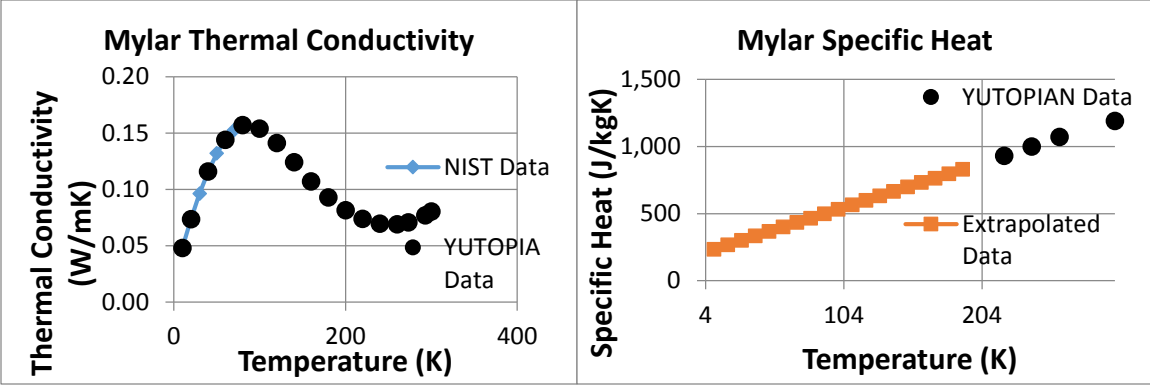
The inaccurate estimation of the band gap using Goldsmid-Sharp analysis creates an interesting opportunity for more analysis. In future iterations of the experiment, it would be useful to compare temperature dependent Seebeck coefficient data with measurements of the effective masses and mobilities of the majority and minority carriers. This dataset would allow for the accuracy of the Seebeck coefficient measurement to be tested. Alternatively, if this dataset disagrees with Goldsmid-Sharp analysis, it would open the door for more interesting analysis and discussion of Goldsmid-Sharp theory.

8. Appendices

Cryogenic properties for brass, copper, mylar, and Teflon (components of the experimental apparatus) are shown below. Data is gathered from National Institute of Standards and Technology (NIST), Engineering Toolbox, and www.yutopian.com/Yuan/prop/Mylar.html

Appendix 1: Cryogenic properties used in COMSOL model





Appendix 2: Cryostat Warming Guidelines

The accuracy of the Seebeck coefficient measurement depends on the experimental apparatus being in thermal equilibrium. It is noted in the methodology section that for each Seebeck coefficient measurement, a temperature set point is entered into the Lakeshore 320 temperature controller, and then ~30 minutes are allowed to pass while the system comes into thermal equilibrium. Attempts to wait less than 30 minutes usually result in an inaccurate Seebeck coefficient measurement. Figure 8-1 shows the temperature measured by both the silicon diode and the Type K thermocouple are shown as a function of time.

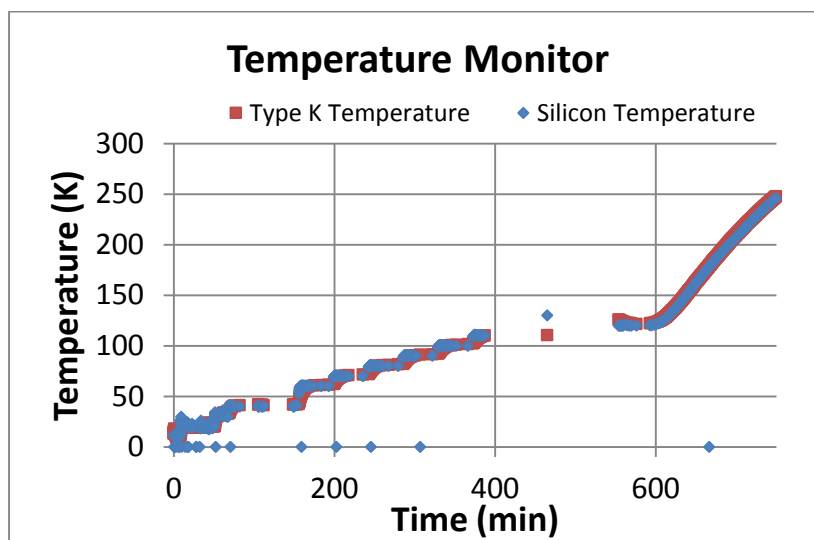


Figure 8-1: Type K temperature and silicon diode temperature of the experimental setup as the cryostat is warmed. At ~400 minutes, the LabView program halted while it prompted the user to turn off the cryopump. At ~600 minutes, the cryostat warmed with the cryopump off. Below ~400 minutes, the incremental adjustment of the temperature set point can be seen. Zeros seen in this graph are a result of dropped communication packets between the Lakeshore 320 and the Labview program.

The voltage measured by the difference Type K thermocouple indicates whether the system is in thermal equilibrium. The difference Type K thermocouple measures the temperature difference between the two copper blocks, not to be confused with the Type K thermocouple that measures the absolute temperature of the cold block (see Methods section). During the Seebeck measurement, the process of heating the hot block creates a temperature difference between the hot and cold blocks. Enough time should be given before beginning another measurement to allow these blocks to come to equilibrium with each other and with the new temperature set point. Figure 8-2 shows the difference thermocouple voltage as a function of time while the experiment is running.

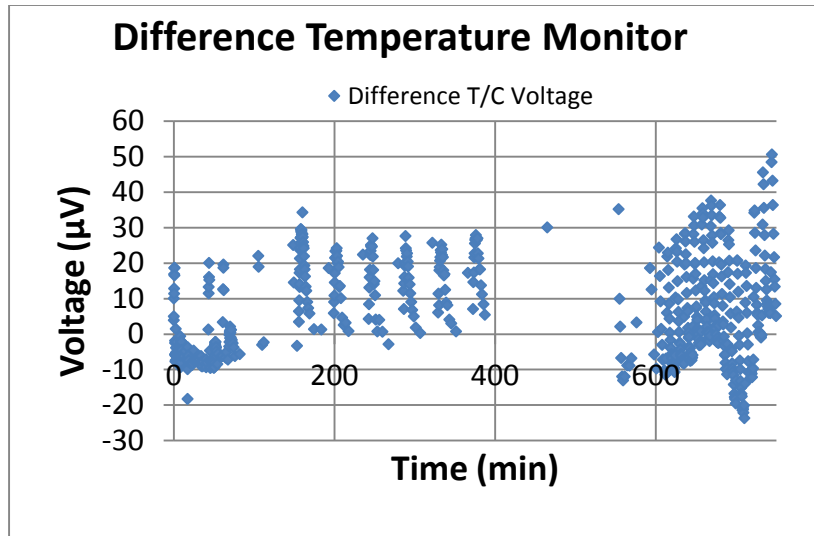


Figure 8-2: The voltage measured by the difference thermocouple as a function of time.

Each peak in Figure 8-2 shows one iteration of the Seebeck coefficient measurement. The important quality to note is that the voltage returns to near zero prior to the beginning of another measurement, indicating the system is in equilibrium and an accurate measurement.

9. Bibliography

1. D. K. Schroder, "Semiconductor Material and Device Characterization", (John Wiley & Sons, Piscataway, NJ, 2006) 3rd Edition
2. T. C. Harman, "Measurement of Pertinent Thermoelectric Properties" I.B. Cadoff and E. Miller, editors, (Reinhold Publishing Cooperation, New York, 1960) Thermoelectric Materials and Devices, Materials Technology Series, Chapter 6, pp. 84-97.
3. T.E. Jenkins, "Semiconductor Science: Growth and Characterization Techniques" (Prentice Hall, New York, 1995)
4. N.W. Ashcroft and N. D. Mermin, "Solid State Physics" (Holt, Rinehart and Winston, New York, 1976)
5. T. Takeuchi, Y. Toyama, and A. Yamamoto, "Role of Temperature Dependent Chemical Potential on Thermoelectric Power" Materials Transactions, **51**, 3 421 (2010).
6. D.K. MacDonad, "Thermoelectricity: An Introduction to the principles" (John Wiley & Sons, Inc. New York, 1962)
7. I. Akihiro, Y. Tomohiro, N. Takayuki, T. Yasushi, T. Sadao, "Seebeck Effects and Electronic Thermal Conductivity of IV-VI Materials" Japanese Journal of Applied Physics **50**, 3 031302 (2011).
8. D. Nemir and J. Beck, "On the Significance of the Thermoelectric Figure of Merit Z" Journal of Electronic Materials, **39**, 9 1897, (2010).
9. Q. Zhu, E.M. Hopper, B.J. Ingram, and T.O. Mason, "Combined Jonker and Ioffe Analysis of Oxide Conductors and Semiconductors" Journal of the American Ceramic Society, **94**, 1 51 (2011).
10. T.M. Tritt and M.A. Subramanian "Thermoelectric Materials, Phenomena, and Applications: A Bird's Eye View" MRS Bulletin, **31**, 3 188 (2006).
11. Material Research Laboratory, UC Santa Barbara. Data accessed February, 2015 <http://www.mrl.ucsb.edu:8080/datamine/thermoelectric.jsp>
12. A.F. Ioffe, "Physics of Semiconductors" (Publishing House of the U.S.S.R., Moscow-Leningrad, 1957) 1st edition.
13. H.J. Goldsmid and J.W. Sharp, "Estimation of the Thermal Band Gap of a Semiconductor from Seebeck Measurements" Journal of Electronic Materials, Vol. 28, Nol. 7, p 870, (1999)
14. Y Goto, Y. Sakai, Y Kamihara, M Matoba, "Effect of Sn-Substitution on Thermoelectric Properties of Copper-Based Sulfide, Famatinite Cu₃SbS₄" Journal of the Physical Society of Japan, 84, 044706, (2015)
15. H. Kim, C.M. Gilmore, A. Piqué, J.S. Horwitz, H. Mattoussi, H. Murata, Z.H. Kafafi, D.B. Chrisey, "Electrical, optical, and structural properties of indium-tin-oxide thin films for organic light-emitting devices" Journal of Applied Physics, 86, 6451, (1999)
16. V. Zeghbroeck, Principles of Semiconductor Devices. Web book, Section 2.8. <http://ecee.colorado.edu/~bart/book/transpor.htm> (2011)